




Efficient removal of formaldehyde with ZIF-8 growth on TiO₂-coated activated carbon fiber felts prepared via atomic layer deposition

Lipei Ren¹, Yan Yu¹, Yuan Yang¹, Qian Zhang¹, Xingfang Xiao^{1,*}, Ruina Liu^{1,*} , and Weilin Xu¹

¹ State Key Laboratory of New Textile Materials and Advanced Processing Technologies, Wuhan Textile University, Wuhan 430073, People's Republic of China

Received: 15 July 2019

Accepted: 17 October 2019

Published online:
8 November 2019

© Springer Science+Business Media, LLC, part of Springer Nature 2019

ABSTRACT

Zeolitic imidazolate framework-8 (ZIF-8) is regarded as an excellent adsorbent material for removing diverse toxic or hazardous gases. However, its milli- to nanoscale size typically restricts its applications. In this study, we demonstrate the ZIF-8 nanocrystals assembled on TiO₂-coated activated carbon fiber felts via atomic layer deposition (ZIF-8@ALD-ACF felts), which can be used as a highly efficient adsorbent for HCHO removal. Using the TiO₂-coated ACF felts as substrates via ALD can provide large number of growth sites for ZIF-8 nanocrystals, which results in fast and highly efficient removal of HCHO. Furthermore, ZIF-8@ALD-ACF felts achieve a highly efficient removal of HCHO under ultraviolet (UV) light. HCHO can be completely removed at high concentration within 110 min. Moreover, under UV light, it can be completely removed at low concentration within 6 min. The micropores in ACF and nanocages in ZIF-8 are suitable for small molecular HCHO uptaking and provide sufficient contact time for photocatalysis by TiO₂. The ALD technology provides a useful methodology for the practical application of MOF-based materials.

Introduction

Metal–organic frameworks (MOFs) are a novel kind of crystalline porous materials self-assembled by metal ions or metal clusters and organic ligands. Due to their large specific surface areas, abundant and adjustable micro-/nanoporous structures, and functional responder loci, MOFs have become one of the

most promising adsorption materials that have attracted considerable attention in recent times [1–4]. Zeolitic imidazolate framework (ZIF-8) is an important MOF fabricated with zinc ions coordinated by four imidazolate rings [5]. They contain small nanopores (0.34 nm) in their structures. Nanoporous structures with diameters of within 2.0 nm exhibit strong van der Waals forces that can effectively

Address correspondence to E-mail: xingfangxiao1@163.com; liuruina26@126.com

adsorb diverse small molecules of toxic or hazardous gases. ZIF-8 also contains larger molecular cages (11.6 nm in diameter) that can also improve adsorption. The specific surface area of ZIF-8 is quite large, and it has a pore volume of approximately $0.63 \text{ m}^3 \text{ g}^{-1}$. ZIF-8 with stable structures can be obtained easily, cheaply, and quickly. Therefore, ZIF-8 is popularly used as an excellent adsorbent material for removing HCHO [6–8]. Long-term exposure to HCHO can cause different diseases such as eye, skin and throat irritation, headache, breathing problems, and even leukemia or cancer [9, 10]. Therefore, removing HCHO is very important to ensure good human health and environmental protection. However, ZIF-8 is typically a milli- to nanoscale crystalline material, which restricts its applications. The loading of nanoscale ZIF-8 on suitable substrates is necessary for practical applications [11, 12].

Nowadays, carbon-based materials, such as activated carbons, activated carbon fibers, and inorganic particles/carbon composite materials, are generally used as HCHO adsorbents [13–16]. The HCHO molecule is very small; hence, physical adsorption on activated carbon usually exhibits low efficiency for HCHO adsorption. Activated carbon fibers have become novel carbon materials with a large specific surface area, several micropores, fast adsorption rate, and nearly no impurity. However, the micropores are in the radial direction with small diffusion resistance; hence, it is easy to achieve HCHO desorption into the air. Functional particles, such as ZIF-8 nanocrystals, loaded on carbon fibers materials can improve the adsorption efficiency [17–19].

Atomic layer deposition (ALD) is a special chemical vapor deposition technique, which is a method of forming thin films by alternately passing a gas-phase precursor pulse through a reaction chamber and a chemical adsorption reaction on the surface of the deposition substrates. Depending on the desired film thickness, multiple repetitions of the growth cycle may be required. ALD technology has been applied in microelectronics, optoelectronics, energy, biology, nanotechnology, catalysis, corrosion resistance, and sealing coating. Some researchers have reported a method known as AIM (ALD in MOFs) that uses ALD to install atomic precision metals into metal-organic frames (MOFs) [20, 21]. They synthesized Zn-AIM-NU-1000 as a catalytical material using the AIM method. Based on this method, we can synthesize

new composites that can catalyze HCHO by ALD (TiO_2) and MOF (ZIF-8) on suitable substrates [22].

Since they combine the advantages of ACF felts and ZIF-8, they can be composited to achieve highly efficient removal of HCHO. Hydrothermal reaction is an efficient and simple method for the growth of ZIF-8 nanocrystals on fiber materials [23, 24]. To achieve higher growth of ZIF-8, the ACF felts can be modified in advance [25–27]. In this study, ACF felts were used as substrates and coated with TiO_2 via ALD. ALD can be employed to make very thin and uniform films of TiO_2 , with the thickness controllable at the atomic level. The structures and properties of the substrates are not affected. In addition, it possesses excellent speed [28–30]. It is propitious for the growth of ZIF-8 nanocrystals; conversely, the HCHO can be photocatalyzed and decomposed into CO_2 and H_2O via TiO_2 under UV light. The HCHO is first captured by the micro-/nanopores in ZIF-8@ALD-ACF felt composite materials and then photocatalyzed via TiO_2 thin film under UV light, given enough contact and decomposition time. It is superior to the adsorption materials that do not compound the fixation and decomposition processes for HCHO. During the adsorption and photocatalysis process, 100% of the HCHO can be removed within 110 min at high concentration and within 6 min at low concentration. The composite material, ZIF-8@ALD-ACF felts, holds important practical applications for HCHO removal.

Experimental

Materials

2-Methylimidazole (2-MeIm) (98% purity) was purchased from MACKLIN. Zinc nitrate hexahydrate ($\text{Zn}(\text{NO}_3)_2 \cdot 6\text{H}_2\text{O}$, 99% purity) and HCHO solution were purchased from Sinopharm Chemical Reagent Co., Ltd of Shanghai (Shanghai, China). Titanium(IV) isopropoxide (TIP, 99.999% metals basis) was obtained from Aladdin Industrial Co., Ltd. Deionized water, purified using a Milli-Q Plus 185 water purification system (Millipore, Bedford, MA), was used throughout this study. The water had a resistivity of 10–16 $\text{M}\Omega \text{ cm}$. Activated carbon fiber felts were purchased from a local market in China. All materials and chemicals were of reagent grade and used without further purification.

Preparation of ZIF-8 nanocrystals

The ZIF-8 nanocrystals were synthesized in purely aqueous solution by integrating the methods reported by Yichang Pan et al. Typically, the molar ratio of $\text{Zn}(\text{NO}_3)_2 \cdot 6\text{H}_2\text{O}$ / 2-methylimidazole/ H_2O in the synthesized solution was set at 1:70:1238 [31]. First, 1.17 g $\text{Zn}(\text{NO}_3)_2 \cdot 6\text{H}_2\text{O}$ and 22.70 g 2-MeIM were dissolved in 8 and 80 ml deionized water, respectively. The two solutions were then mixed by mechanical stirring. Subsequently, the mixture was transferred to a Teflon-lined autoclave and hydrothermally reacted at 70 °C for 24 h. The final ZIF-8 nanocrystals were collected by centrifuging at 8000 r min^{-1} for 15 min, adequately washed with ethanol and deionized water, and then dried at 50 °C.

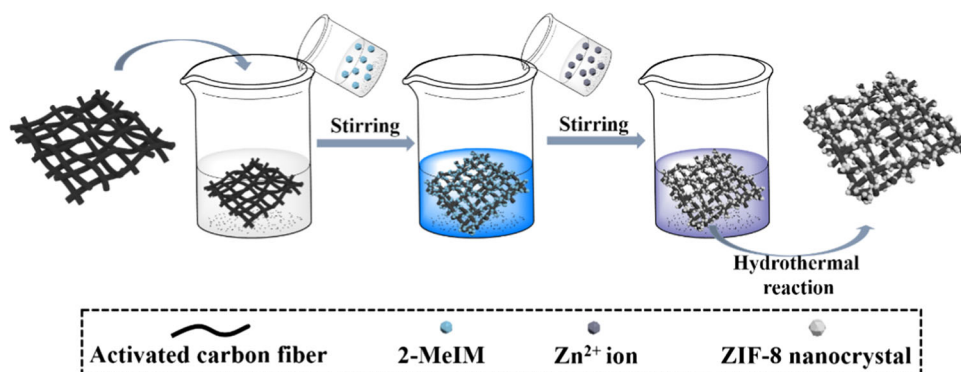
Preparation of ZIF-8-coated activated carbon fiber felts (ZIF-8@ACF felts)

The ZIF-8 @ ACF felts composite was prepared under the same conditions. The procedure for preparing ZIF-8-coated activated carbon fiber felts is presented in Fig. 1. First, 3 g activated carbon fiber felts were added to the solution of 22.70 g 2-MeIM 80 ml deionized water and moderately stirred for 5 min. Then, a solution of 1.17 g $\text{Zn}(\text{NO}_3)_2 \cdot 6\text{H}_2\text{O}$ in 8 ml deionized water was added into the reaction system drop by drop. After stirring moderately for another 5 min, the mixture was transferred to a Teflon-lined autoclave and hydrothermally reacted at 70 °C for 24 h. The final ZIF-8 @ ACF felts samples were adequately washed with ethanol and deionized water and then dried naturally.

Preparation of ZIF-8 nanocrystals growth on TiO_2 -coated activated carbon fiber felts via ALD (ZIF-8@ALD-ACF felts)

The process for preparing TiO_2 -coated activated carbon fiber felts via ALD was conducted using a Savannah S100 ALD reactor (Savannah System, Cambridge NanoTech. Inc., USA) equipped with a gas-flow system. Titanium(IV) isopropoxide and H_2O were used as titanium and oxygen precursors, respectively, to deposit TiO_2 at a temperature of 150 °C. High-purity nitrogen (N_2 , 99.999%) was used as both purge gas and carrier gas for both precursors. A steady flow of nitrogen at 50 sccm (standard cubic centimeters per minute) was used in the ALD process. Prior to the ALD processing, the activated carbon fiber felts were placed in the ALD reactor and dried in vacuum (~ 0.5 Torr) at 150 °C for 5 min. To produce adequate vapor pressures, the TIP was heated to 80 °C and the water was maintained at the ambient temperature. In the first half cycle, water vapor was pulsed into the chamber for 0.05 s, the activated carbon fiber felts were exposed to water vapor for 8 s; the reactor was then purged with nitrogen for 20 s. In the second half cycle, TIP was pulsed into the chamber for 0.2 s, the activated carbon fiber felts were exposed to TIP for 8 s, and the reactor was purged with nitrogen for 20 s. Each complete ALD cycle lasted for a duration of 56.25 s [32]. The TiO_2 -coated ACF felts used in this work were processed 1000 cycles. The hydrothermal method employed is the same as the above; however, the activated carbon fiber felts were replaced with TiO_2 -coated activated carbon fiber felts as substrate. The ZIF-8@ALD-ACF felts were obtained, and the entire process is shown in Fig. 2.

Figure 1 Schematic showing the preparation procedure for ZIF-8-coated activated carbon fiber felts.



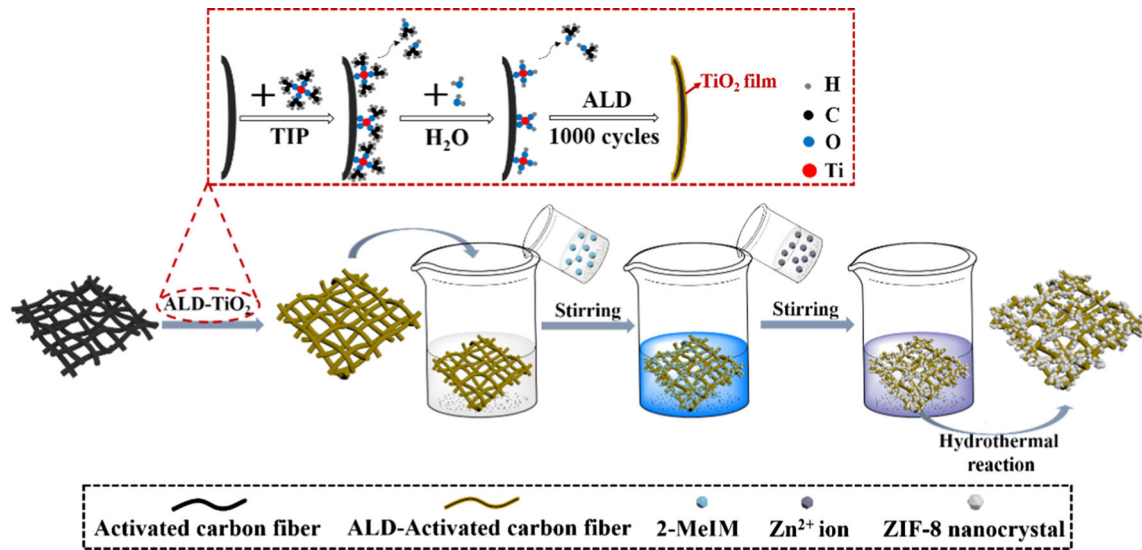


Figure 2 Schematic diagram showing the process for TiO_2 -coated on ACF felts via ALD and ZIF-8 nanocrystals growth on ALD-ACF felts.

Characterization

The magnetic suspension balance, RUBOTHERM, with a precision of 0.0001 g was supplied by Germany. Morphologies of the ACF felts, 1000 cycles of ALD-ACF felts, ZIF-8@ACF felts, and ZIF-8@ALD-ACF felts were examined on a scanning electron microscope (JSM-5610LV, JEOL Co. Ltd, Japan) at 15 kV after gold coating. X-ray diffraction (XRD) was performed at room temperature using an X'Pert PRO XRD spectrometer (PANalytical, Holland) with a $\text{Cu-K}\alpha$ radiation source at a generator voltage of 40 kV and a generator current of 50 mA. The changes in the formaldehyde adsorbed by activated carbon fiber felt station was measured by Bruker Tensor 27 Fourier-transform infrared spectroscopy (FT-IR). The adsorbate for this study was HCHO solution purchased from Sinopharm Chemical Reagent Co., Ltd., with 99.0% purity. The HCHO standard solution was heated at a certain temperature before placing it inside the test chamber. The HCHO adsorption and catalysis tests are static at room temperature (25 °C), and the relative humidity was about 40%–60%. HCHO at high concentration (100 mg m^{-3}) or low concentration (10 mg m^{-3}) was used as an initial concentration in a test chamber having a volume of 0.5 m^3 . The mass of adsorbents (ACF, ALD-ACF, ZIF-8@ACF, and ZIF-8@ALD-ACF felts) was 3 g. At the beginning of the experiment, the corresponding HCHO concentration was recorded per minute.

Results and discussion

Structure and morphology of the ZIF-8 nanocrystals, ACF felts, ALD-ACF felts, ZIF-8@ACF felts, and ZIF-8@ALD-ACF felts

The morphology and microstructure of the pure ZIF-8 nanocrystals were examined using SEM and XRD. Figure 3a reveals that ZIF-8 particles exhibit hexagonal and cube-like shape ca. 100 nm in diameter. The XRD patterns of pure ZIF-8 nanocrystals are shown in Fig. 3b. ZIF-8 nanocrystal peaks at $2\theta = 7.3^\circ, 10.4^\circ, 12.7^\circ, 14.7^\circ, 16.4^\circ,$ and 17.9° are associated with the crystal planes (011), (022), (112), (022), (013), and (222) of the ZIF-8 nanocrystals, respectively [33]. All observed peaks fairly matched the standard XRD pattern of ZIF-8 from the CCDC file (602542). The ZIF-8 nanocrystals were synthesized in a purely aqueous solution. The nanoparticles obtained can be suitably dispersed in deionized water to form a stable suspension and can be kept for several days without settling (the inset in Fig. 3a).

The morphology and microstructure of the ACF felt, ALD-ACF felts, ZIF-8@ACF felts, and ZIF-8@ALD-ACF felts are shown in Fig. 4. ACF felts (Fig. 4a, b) and ALD-ACF felts (Fig. 4d, e) were clean with relatively smooth textures. The ALD process produces very thin and uniform films of TiO_2 with smooth fibers surfaces. After the hydrothermal reaction, nanoscale ZIF-8 was coated on ACF felts or ALD-ACF felts. Some ZIF-8 crystalline particles could

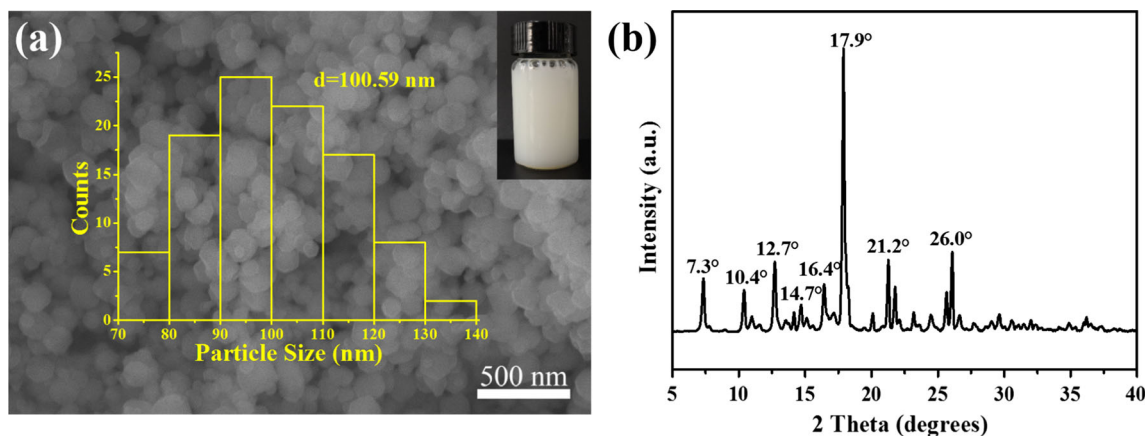


Figure 3 **a** SEM images of pure ZIF-8 nanocrystals; the inset represents corresponding particle size distributions and a digital photograph of an opalescent stable suspension of the as-

synthesized ZIF-8 nanocrystals dispersed in deionized water. **b** XRD patterns of pure ZIF-8 nanocrystals.

be observed to be coated on the ACF felts (Fig. 4g, h). However, it can be reached easily from relatively sparse ZIF-8 crystalline particles on ACF felts to dense ZIF-8 crystalline film on ALD-ACF felts (Fig. 4j, k). More active growth sites can be provided for ACF felts as substrates by TiO_2 via ALD, which is beneficial to the coating of ZIF-8.

Results of the EDS analyses conducted to determine the chemical composition of ACF felts, ALD-ACF felts, ZIF-8@ACF felts, and ZIF-8@ALD-ACF felts are illustrated in Fig. 4c, f, i, l. Only carbon, oxygen, and platinum were detected in the spectra of the ACF felts. The presence of platinum can be attributed to the coating layer used for the EDS measurement, while the presence of carbon and oxygen can be attributed to the ACF felts. After the ALD processing, elements such as carbon, oxygen, and platinum were found in the EDS spectra. No other elements, except titanium, were found in the EDS spectra, hence confirming that Ti is present on the surfaces of ALD-ACF felts and ZIF-8@ALD-ACF felts. Meanwhile, after the hydrothermal reaction, in the ZIF-8@ACF felts and ZIF-8@ALD-ACF felts samples, zinc element was found in the EDS spectra, indicating that ZIF-8 crystalline film was coated on the ACF felts and ALD-ACF felts.

Figure 5a shows the FT-IR spectra of the adsorbents, ZIF-8@ACF felts, and ZIF-8@ALD-ACF felts; nearly all the FT-IR bands are consistent with those of the previously reported ZIF-8. The bands at $2916\text{--}3170\text{ cm}^{-1}$ can be attributed to the aromatic and aliphatic C-H stretch of the imidazole. C=N stretching could be observed at 1590 cm^{-1} . The imidazole

ring out-of-plane bending vibrations result in absorption bands below 800 cm^{-1} , such as peaks at $680, 745\text{ cm}^{-1}$, while bands due to in-plane bending vibrations can be observed in the range of $900\text{--}1350\text{ cm}^{-1}$, such as peaks at 1310 and 1110 cm^{-1} . The bands at $1350\text{--}1500\text{ cm}^{-1}$ are associated with the entire imidazole stretching, such as a peak at 1432 cm^{-1} due to the effects of imidazole ring stretching or bending [14, 34, 35]. Figure 5b shows XRD patterns of the ACF felts, ALD-ACF felts, ZIF-8@ACF felts, ZIF-8@ALD-ACF felts, and ZIF-8 nanocrystals. As shown in Fig. 5b, the ACF felts exhibited characteristic peaks at $2\theta = 24.5^\circ$ and $2\theta = 3.5^\circ$, indicating the coexistence of ACF felts I and ACF felts II structures. The peaks at $2\theta = 24.5^\circ$ and $2\theta = 43.5^\circ$ were also observed in the XRD patterns of ALD-ACF felts subjected to 1000 ALD cycles, but the intensity of the peaks was not as high as those for pure ACF felts, indicating that the amount of ACF felts I crystalline structure in the ALD-ACF felts was less than the amount in the ACF felts. It should be noted that there are no typical diffraction peaks for the rutile and/or anatase TiO_2 structures on the ALD 1000 cycles-ACF felts. However, individual TiO_2 replica exhibited an anatase structure with preferred (101) orientation, indicating that the ALD coating on the silk fabrics was TiO_2 and that the crystal structure was an amorphous structure [33]. The ZIF-8@ACF felts and ZIF-8@ALD-ACF felts peaks at $2\theta = 7.3^\circ, 10.4^\circ, 12.7^\circ, 14.7^\circ, 16.4^\circ, \text{ and } 17.9^\circ$ were associated with characteristic peaks of ZIF-8 nanocrystals, indicating the abundant existence of ZIF-8 nanocrystals

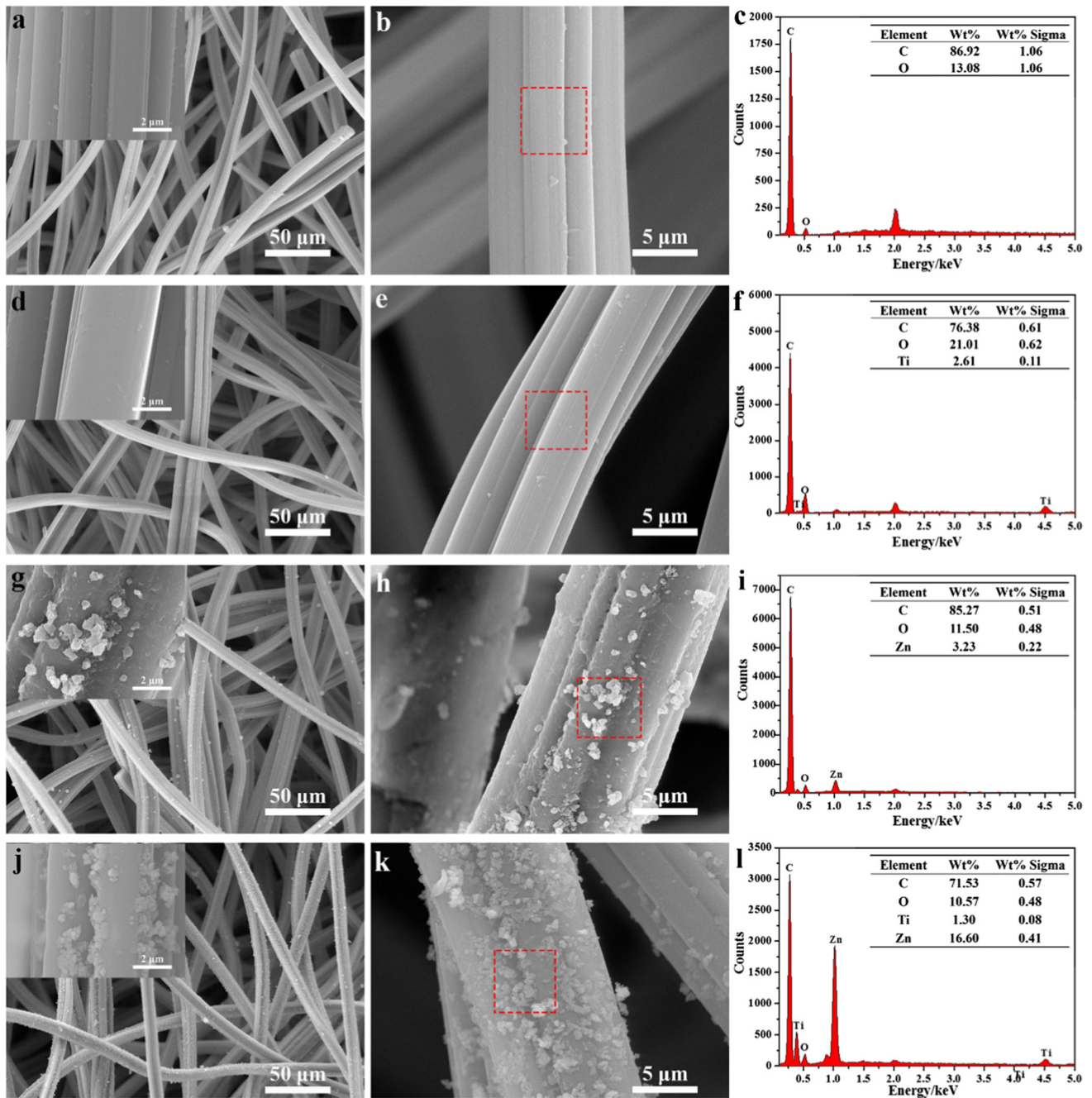


Figure 4 SEM images and EDS spectra of the adsorbents: **a–c** ACF felts, **d–f** ALD-ACF felts, **g–i** ZIF-8@ACF felts, **j–l** ZIF-8@ALD-ACF felts.

in the network of ZIF-8@ACF felts and ZIF-8@ALD-ACF felts.

The content of ZIF-8 coated on the ACF or ALD-ACF felts was determined using the weighing method. The detailed data are shown in Table 1. The possible mechanisms for the growth of ZIF-8 nanocrystals on the surface of ACF felts and ALD-ACF felts are shown in Fig. 5c. The growth of ZIF-8

on the surface of fibers can be explained by two mechanisms: coordination interactions and electrostatic interactions. As shown in Fig. 5c I, after the addition of Zn^{2+} in the ACF felts or ALD-ACF felts, the Zn^{2+} ions interact with the $-\text{O}$ or $-\text{OH}$ groups existing on ACF felts or ALD-ACF felts surface by coordination. The bonded Zn^{2+} facilitates the nucleation of ZIF-8, thus leading to the immobilization of

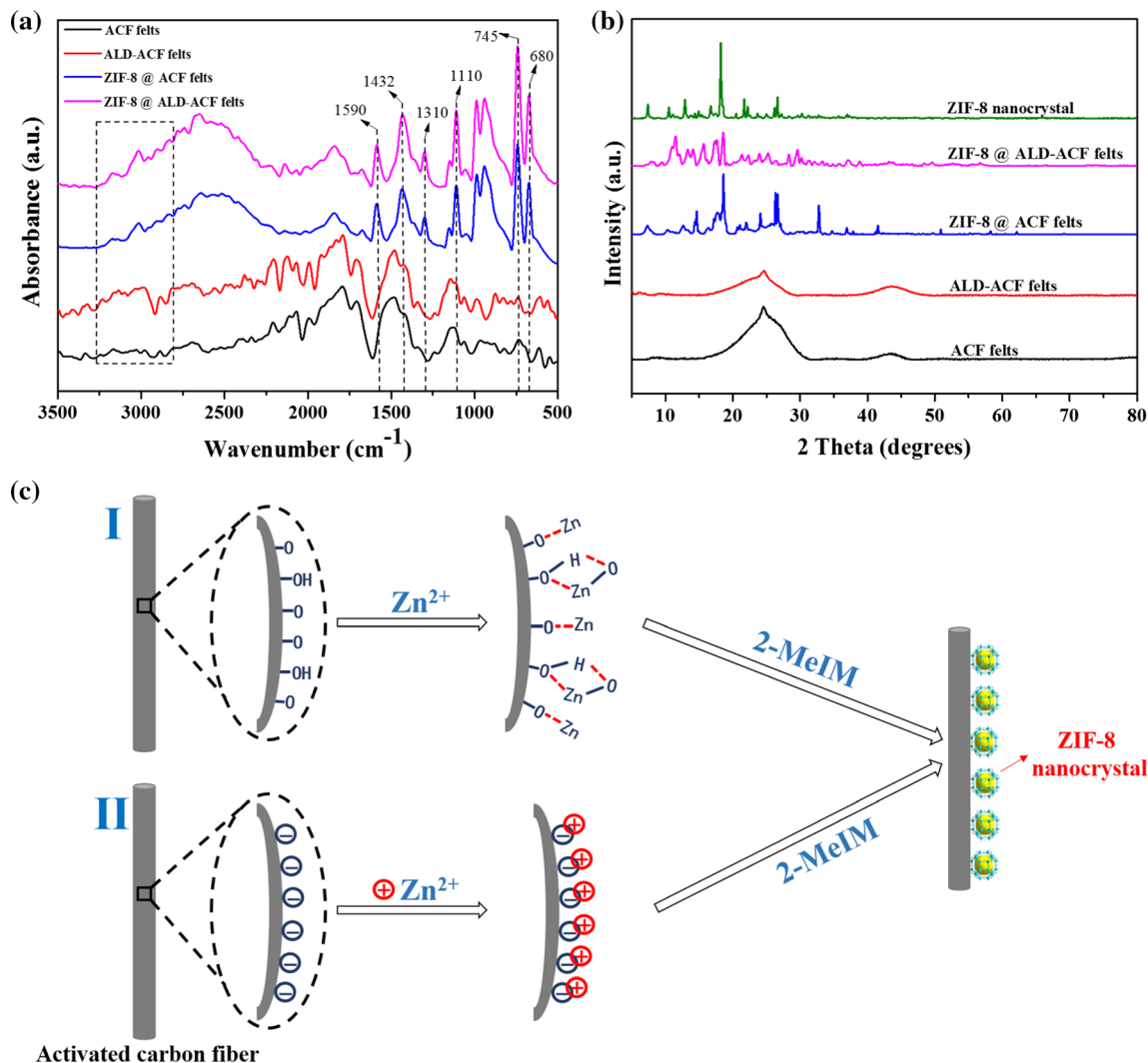


Figure 5 a FT-IR spectra of the adsorbents: ACF felts, ALD-ACF felts, ZIF-8@ACF felts, and ZIF-8@ALD-ACF felts. b XRD patterns of the ACF felts, ALD-ACF felts, ZIF-8@ACF felts, ZIF-8@ALD-ACF felts, and ZIF-8 nanocrystals. c Possible

mechanisms (I) coordination interactions, (II) electrostatic interactions, for the growth of ZIF-8 nanocrystals on the surface of ACF felts or ALD-ACF felts.

Table 1 The mass of ZIF-8 coated on different samples

Adsorbents	The mass of adsorbents before ZIF-8 coating (g)	The mass of adsorbents after ZIF-8 coating (g)	The mass of ZIF-8 load (g)
ACF felts	1.00	/	/
ALD-ACF felts	1.00	/	/
ZIF-8@ACF felts	1.00	2.03	1.03
ZIF-8@ALD-ACF felts	1.00	2.54	1.54

the generated ZIF-8 nanocrystals on the surface of the ACF felts or ALD-ACF felts [36–38]. In addition, as shown in Fig. 5c II, the surface of the ACF felts or

ALD-ACF felts is electronegative in aqueous solutions. Once the Zn²⁺ sites for 2-methylimidazole molecules, finally resulting in the generated ZIF-8

nanocrystals were attached on the surface of ACF or ALD-ACF felts [33, 39]. Due to the TiO₂ coated on the surface of the ACF felts, the coordination sites and charge numbers are greater than those of ACF felts. This is propitious to the growth of ZIF-8 nanocrystals.

The porous features and Brunauer–Emmett–Teller (BET) analysis of the ZIF-8 nanocrystals, ZIF-8@ACF, and ZIF-8@ALD-ACF felts were investigated using nitrogen isothermal adsorption/desorption measurements. In Fig. 6, ZIF-8 shows a type-II isotherm, whereas the isotherms of ZIF-8@ACF and ZIF-8@ALD-ACF felts have the type-III shape with the H₃ hysteresis loop (relative pressure ranging from 0.5 to 0.98; Fig. 6a), indicating both the micropore and mesopore structure of ZIF-8@ACF and ZIF-8@ALD-ACF felts. The corresponding specific surface areas of ZIF-8 nanocrystals, ZIF-8@ACF, and ZIF-8@ALD-ACF felts were determined to be 1278.75, 792.18, and 868.51 m² g⁻¹, respectively. The specific surface area of ZIF-8@ALD-ACF felts was found to be greater than that of the ZIF-8@ACF felts, which is favorable for the diffusion of HCHO molecules; this is also beneficial for the photocatalytic reaction by TiO₂ thin film [30, 32, 40]. The pore width distribution in Fig. 6b also indicates that more micro-/mesopores exist in ZIF-8@ALD-ACF felts, which complies with both the total pore volume and surface area of pores as shown in Table 2.

HCHO adsorption by the ACF felts, ALD-ACF felts, ZIF-8@ACF felts, and ZIF-8@ALD-ACF felts without UV light

The effect of initial HCHO concentration on the removal percentage was conducted with different initial concentrations (high HCHO concentration: 100 mg m⁻³ and low HCHO concentration: 10 mg m⁻³) in the test chamber. The amount of adsorbent was fixed and exposed to high HCHO concentration (100 mg m⁻³) in the test chamber for 2 h, with the data read at minute intervals. The removal efficiency of HCHO was calculated using Eq. 1. The adsorption capacity was evaluated using Eq. 2. The adsorption test for low HCHO concentration was performed in a similar manner. A given amount of adsorbent was exposed to a low concentration of HCHO until the amount of HCHO was adsorbed to zero; the adsorption time was then compared.

$$\text{Removal efficiency (\%)} = \frac{C_0 - C_t}{C_0} \times 100\% \quad (1)$$

$$\text{Adsorption capacity, } q_t (\text{mg g}^{-1}) = \frac{C_0 - C_t}{M} \times V \quad (2)$$

where C_0 represents the initial concentration of HCHO in the test chamber (mg/m³) at time, $t = 0$; C_t represents the concentration of HCHO at time = t (1, 2, 3 until 120 min); q_t represents the HCHO adsorption capacity at time = t (1, 2, 3 until 120 min); M represents the weight of the adsorbent (g), and V represents the volume of the test chamber (m³).

The removal percentage of HCHO by different adsorbents (ACF felts, ALD-ACF felts, ZIF-8@ACF

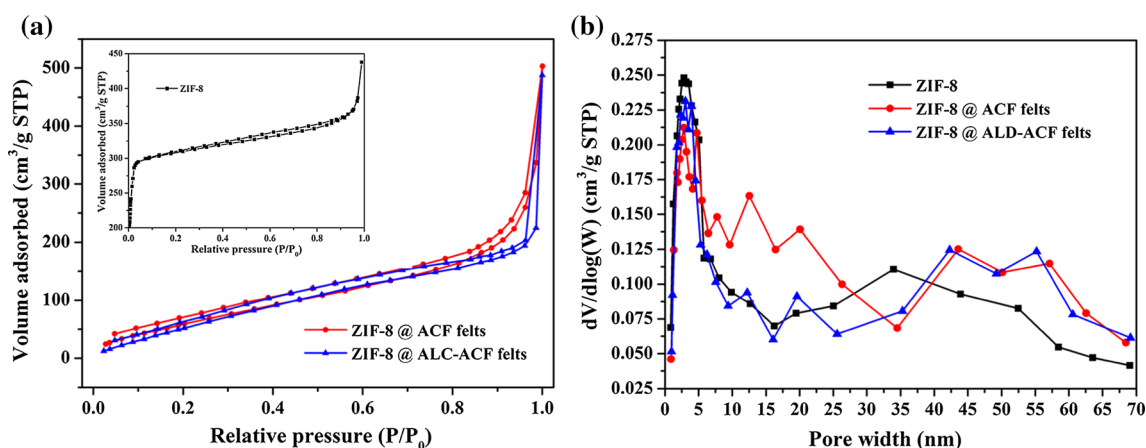


Figure 6 **a** Nitrogen adsorption–desorption isotherms and **b** pore size distributions of ZIF-8, ZIF-8@ACF, and ZIF-8@ALD-ACF felts. P the gas-phase pressure when adsorption equilibrium was achieved; P_0 the saturated vapor pressure; V the volume; and W the width.

Table 2 Porous structure of the samples evaluated by N_2 adsorption

Samples	S_{BET} ($m^2 g^{-1}$)	Pore volume ($cm^3 g^{-1}$)	Average pore size (nm)
ZIF-8	1278.75	0.65	1.97
ZIF-8@ACF felts	792.18	0.27	7.92
ZIF-8@ALD-ACF felts	868.51	0.29	6.29

felts, ZIF-8@ALD-ACF felts) at high HCHO concentrations is shown in Fig. 7a. The removal rate is rapid within the first 20 min; it then rises gradually until it reaches the adsorption equilibrium at 120 min. The maximum HCHO removal efficiency is 78.02% for ACF felts, 79.51% for ALD-ACF felts, 95.36% for ZIF-8@ACF felts, and 99.01% for ZIF-8@ALD-ACF felts (Fig. 7b). The removal efficiencies for HCHO by ACF felts and ALD-ACF felts are about the same. The TiO_2 forms a very thin film on the surface of the ACF via ALD, which does not have an obvious effect on the micropore structures of the ACF for HCHO adsorption. The growth of ZIF-8 nanocrystals on ACF felts

significantly improves the removal efficiency. Using ALD-ACF felts as substrate provides more growth sites, and the amount of ZIF-8 nanocrystals is greater than those of the ACF felts substrate. The nanoporous and molecular cage structures in ZIF-8 are favorable for HCHO adsorption. Therefore, using ZIF-8@ALD-ACF felts as adsorbent offers the highest removal efficiency (above 99%). The curves of adsorption capacity vs. time for ZIF-8@ACF felts and ZIF-8@ALD-ACF felts are shown in Fig. 7c, d. The maximum HCHO adsorption capacity is 14.812 and 15.408 $mg g^{-1}$ for ZIF-8@ACF felts and ZIF-8@ALD-ACF felts using 120 min. They both suitably fit the

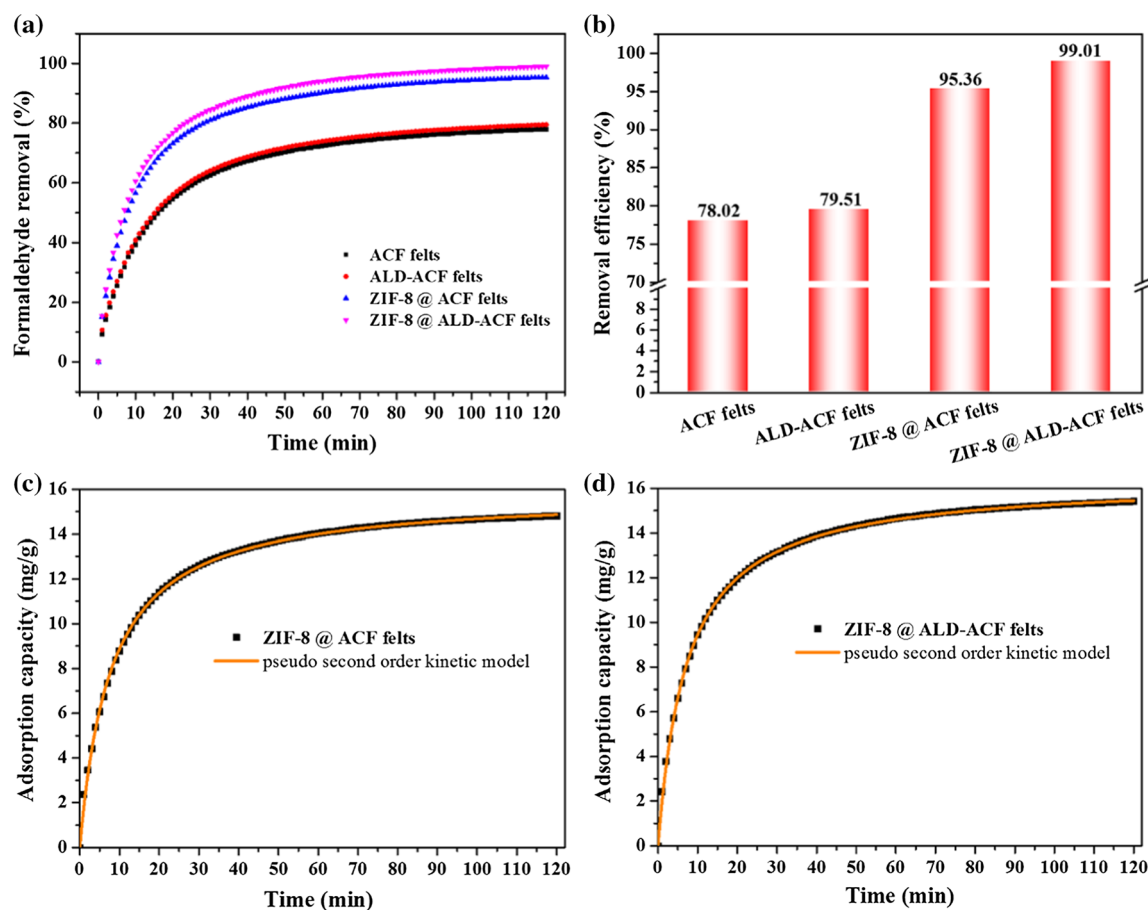


Figure 7 a Percentage of HCHO removal at high concentration using different adsorbents, b column diagram of the adsorption efficiency, c adsorption capacity of ZIF-8@ACF felts and the

pseudo-second-order kinetic model, d adsorption capacity of ZIF-8@ALD-ACF felts and the pseudo-second-order kinetic model.

pseudo-second-order kinetic model. The pseudo-second-order kinetic model is evaluated using Eq. 3.

$$\text{Adsorption capacity, } q_t(\text{mg g}^{-1}) = \frac{k_2 q_e^2 t}{1 + k_2 q_e t} \quad (3)$$

where k_2 represents the pseudo-secondary adsorption rate constant and q_e represents the equilibrium adsorption capacity. In Fig. 7c, the fitting equation is given by $q_t = \frac{0.00804 \times 15.838^2 \times t}{1 + 0.00804 \times 15.838 \times t}$ ($R^2 = 0.999$), and in Fig. 7d, $q_t = \frac{0.00829 \times 16.397^2 \times t}{1 + 0.00829 \times 16.397 \times t}$ ($R^2 = 0.999$).

The percentage of HCHO removal using different adsorbents (ACF felts, ALD-ACF felts, ZIF-8@ACF felts, ZIF-8@ALD-ACF felts) at low HCHO concentration (10 mg/m^3) is also studied. As shown in Fig. 8, the four adsorbents can all remove HCHO completely from the test chamber. ZIF-8@ALD-ACF felts have a rapid rate of HCHO removal at low concentration, leading to full adsorption of the HCHO in less than 8 min. ZIF-8@ACF felts come second, taking 13 min to ensure full adsorption of the HCHO. The slowest are untreated ACF felts and ALD-ACF felts, which take 16 min. The reason is the same as the above.

HCHO removal by the ACF felts, ALD-ACF felts, ZIF-8@ACF felts, and ZIF-8@ALD-ACF felts under UV light

The percentage of HCHO removal by adsorbents (ACF felts, ALD-ACF felts, ZIF-8@ACF felts, ZIF-8@ALD-ACF felts) at high HCHO concentrations under UV light is shown in Fig. 9a. Figure 9b shows a column diagram of their adsorption efficiencies. It

can be observed from the figure that ZIF-8@ALD-ACF felts exhibit the highest removal efficiency at high HCHO concentration, achieving 100% removal at 110 min. ZIF-8@ACF felts come in second place (96.88%), while ALD-ACF felts come third (89.02%). The worst performance comes from untreated ACF felts that achieve only 78.01%.

The efficiencies of removal of ACF felts and ZIF-8@ACF felts are nearly no change with or without UV light. The efficiencies of removal of ALD-ACF felts and ZIF-8@ALD-ACF felts still clearly increase under the condition that the adsorption time is shortened by 10 min. This is mainly due to the photocatalysis of the TiO_2 . Adsorbents without TiO_2 adsorb HCHO molecules due to their micro-/nanopores and large specific surface area. In contrast, adsorbents containing TiO_2 capture first HCHO molecule, and then decompose it to CO_2 and H_2O using TiO_2 under UV light. The process can also be observed from the curve of ZIF-8@ALD-ACF felts in Fig. 9a. A turning point can be clearly observed at 70 min. Before 70 min, the ZIF-8@ACF felts and ZIF-8@ALD-ACF felts exhibit similar adsorption behavior under UV light. From 70 min, photocatalysis of the TiO_2 is dominant for HCHO decomposition. The amount of HCHO in the test chamber was completely removed.

The adsorption capacity of ZIF-8@ACF felts and ZIF-8@ALD-ACF felts under UV light is shown in Figs. 9c, d. The maximum HCHO adsorption capacity is 15.056 and 15.559 mg g^{-1} for ZIF-8@ACF felts and ZIF-8@ALD-ACF felts, respectively. In Fig. 9c, the curve of ZIF-8@ACF felts is consistent with the pseudo-second-order kinetic model. The fitting

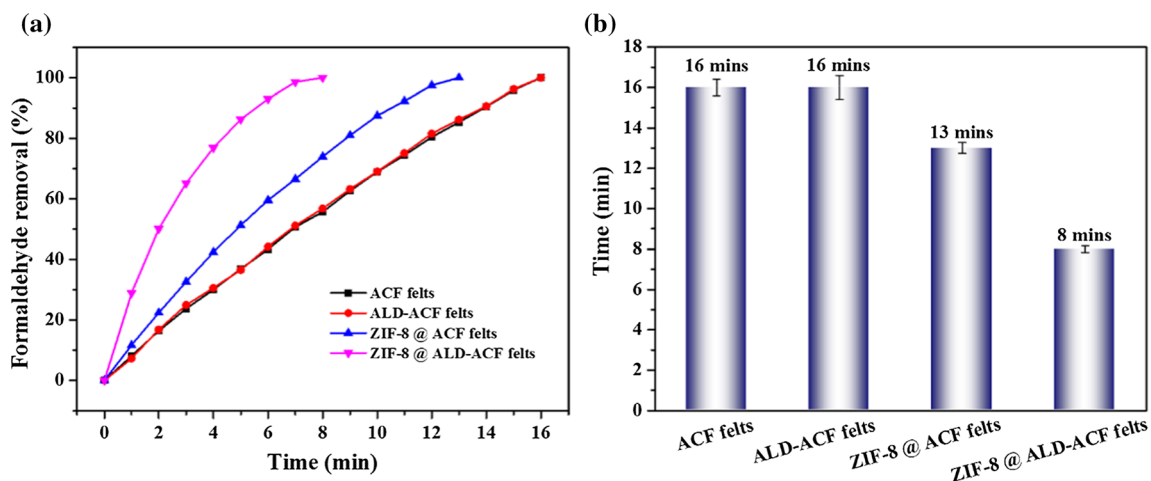


Figure 8 HCHO removal at low concentration using different adsorbents **a** and column diagram of their adsorption time **b**.

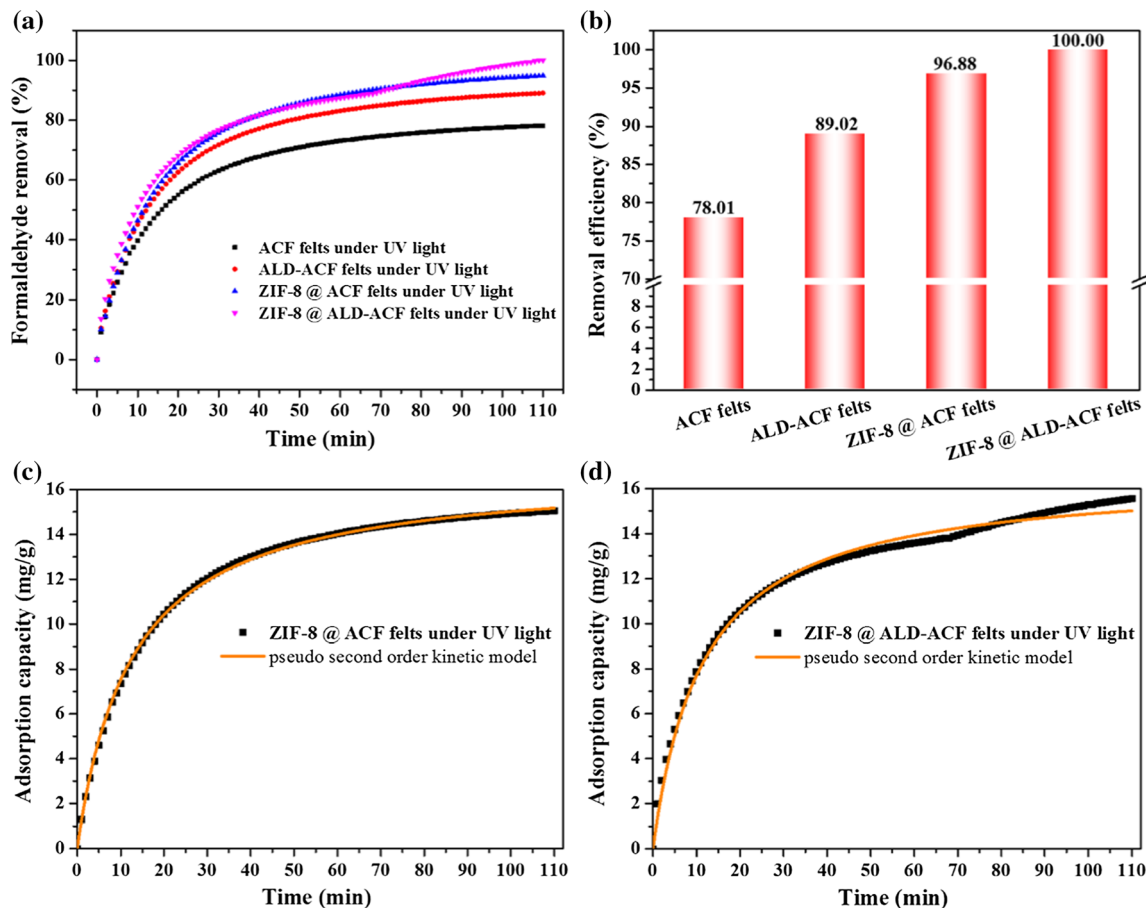


Figure 9 a Percentage of HCHO removal at high concentration using different adsorbents under UV light within 110 min, b column diagram of their adsorption efficiencies, c adsorption capacity of ZIF-8@ACF felts and the pseudo-second-order kinetic

model under UV light, (d) adsorption capacity of ZIF-8@ALD-ACF felts and the pseudo-second-order kinetic model under UV light.

equation is given by $q_t = \frac{0.00475 \times 16.891^2 \times t}{1 + 0.00475 \times 16.891 \times t}$ ($R^2 = 0.999$). In Fig. 9d, due to the turning point, the curve does not fit the pseudo-second-order kinetic model very well; hence, $q_t = \frac{0.00523 \times 16.584^2 \times t}{1 + 0.00523 \times 16.584 \times t}$ ($R^2 = 0.992$).

The percentage of HCHO removal for adsorbents (ACF felts, ALD-ACF felts, ZIF-8@ACF felts, ZIF-8@ALD-ACF felts) at low HCHO concentrations under UV light is shown in Fig. 10. The figure shows that four different adsorbents can all remove HCHO completely from the test chamber. ZIF-8@ALD-ACF felts exhibit the fastest rate of removal of HCHO under UV light, achieving total removal in less than 6 min. ZIF-8@ACF felts as adsorbent come second, achieving total removal in 13 min. ALD-ACF felts come third at 14 min, while the slowest are untreated ACF felts that take 16 min. Compared to the adsorption conditions without UV light irradiation, there are also no influences on ACF felts and ZIF-

8@ACF felts. Due to the photocatalysis of TiO_2 under UV light, the adsorption times were shortened and the adsorption efficiencies of ZIF-8@ALD-ACF felts and ALD-ACF felts that both contain TiO_2 thin films via ALD were significantly improved.

Figure 11 shows the mechanism of HCHO removal. The surface of the ACF is smooth and inert, making the growth of ZIF-8 nanocrystals on the fibers difficult. As can be seen from the SEM images and local magnification, the ACF surface became rough with sparse ZIF-8 nanocrystals. When the ACF was coated in advance with TiO_2 thin film via ALD, a dense and uniform growth of nanocrystals on the ACF was observed. ALD makes the thickness of TiO_2 thin film controllable at the atomic level. The speed of the reaction between ACF and TiO_2 is excellent and does not affect the structures and properties of the ACF substrates. In addition, the TiO_2 can provide

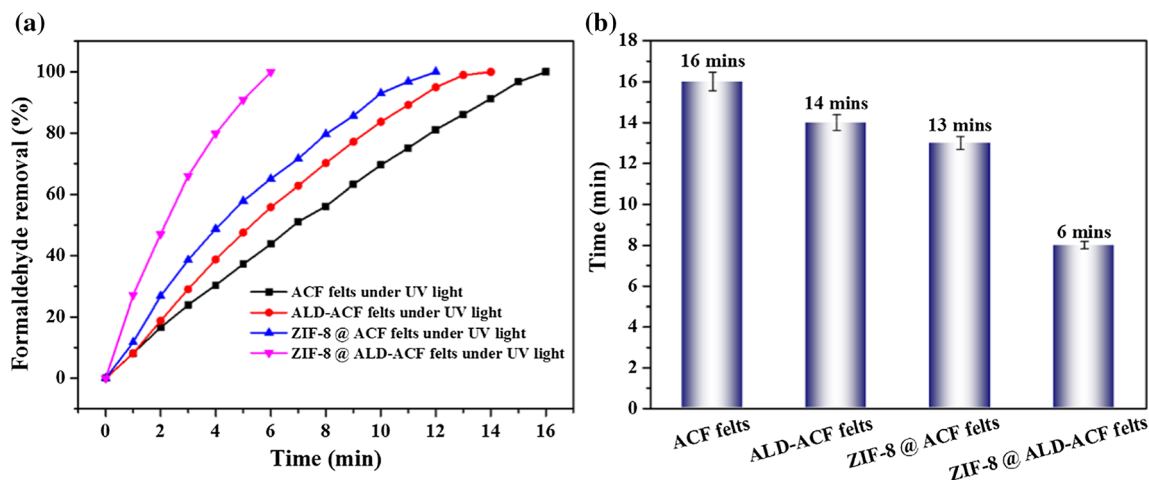


Figure 10 Removal percentage at low HCHO concentration for different adsorbents under UV light (a) and column diagram of their adsorption time (b).

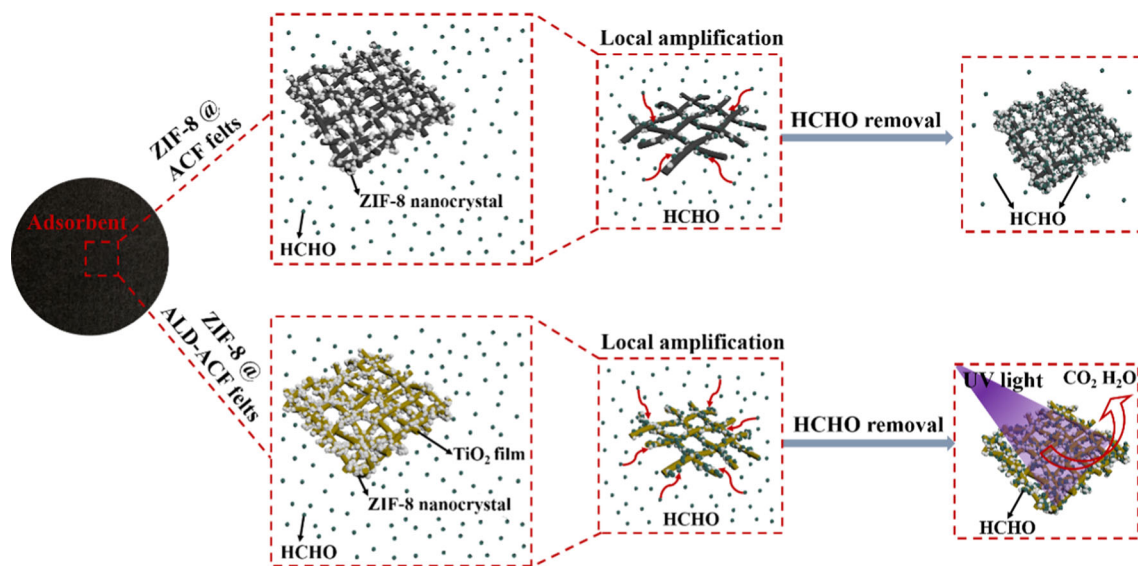


Figure 11 Mechanism of HCHO removal for ZIF-8@ACF felts and ZIF-8@ALD-ACF felts under UV light.

more binding sites for the growth of ZIF-8. The nanopores and cage structures of ZIF-8 are propitious for adsorbing and fixing HCHO molecules. Due to the synergistic reaction of ZIF-8 and ACF felts, the ZIF-8@ACF felts and ZIF-8@ALD-ACF felts both achieve high HCHO adsorption efficiency (95.36% and 99.01%) without UV light. A large number of HCHO molecules are first captured by the composite materials on the surface of fibers and ZIF-8, in the nanopores and molecular cages, and in the micropores formed after compounding. In particular, the nanopores exhibit strong van der Waals forces that can effectively adsorb very small HCHO molecules and prevent desorption. When the adsorption

equilibrium is reached, a very small amount of HCHO molecules are still left in the test chamber (the upper part of Fig. 11). Under UV light, the HCHO molecules are first captured by ZIF-8@ALD-ACF felts. Then, the HCHO molecules have sufficient time to contact the TiO₂ thin film and decompose to CO₂ and H₂O [41–45]. They can be completely removed even within several minutes. The capture–sufficient contact–decomposition process employed in this study is very effective and practical for HCHO removal. The method can also effectively avoid secondary pollution and has wide application prospects.

Conclusion

In this study, we successfully prepared novel ZIF-8@ALD-ACF felts composite materials. These ZIF-8@ALD-ACF felts can be used as a highly efficient adsorbent for HCHO. Using TiO₂-coated ACF felts via ALD as substrates can provide more growth sites for ZIF-8 nanocrystals and HCHO photocatalytic degradation. The adsorption and photocatalytic processes can be mainly described as the capture-sufficient contact-decomposition process. The felts achieve 100% removal of HCHO at high concentration within 110 min and 100% removal at low concentration within 6 min under UV light. Providing a sufficient contact time between HCHO and TiO₂ thin film, HCHO captured and fixed in the micro-/nanopores of the ZIF-8@ALD-ACF felts is decomposed into CO₂ and H₂O. Hence, the process can effectively prevent secondary pollution. The ZIF-8@ALD-ACF felts composite materials hold important practical applications for HCHO removal.

Acknowledgments

This work was financially supported by the National Natural Science Foundation of China (Grant Numbers 51502208 and 51325306) and the China Scholarship Council (Grant Number 201608420039).

References

- [1] Allendorf MD, Bauer CA, Bhakta RK, Houk RJT (2009) Luminescent metal-organic frameworks. *Chem Soc Rev* 38:1330–1352
- [2] Wang B, Xie LH, Wang X et al (2018) Applications of metal-organic frameworks for green energy and environment: New advances in adsorptive gas separation, storage and removal. *Green Energy Environ* 3:191–228
- [3] Zhang Y, Yuan S, Feng X et al (2016) Preparation of nanofibrous metal-organic-framework filters for efficient air pollution control. *J Am Chem Soc* 138:5785–5788
- [4] Barea E, Montoro C, Navarro JAR (2014) Toxic gas removal metal-organic frameworks for the capture and degradation of toxic gases and vapours. *Chem Soc Rev* 43:5419–5430
- [5] Fairen-Jimenez D, Moggach SA, Wharmby MT et al (2011) Opening the gate: framework flexibility in ZIF-8 explored by experiments and simulations. *J Am Chem Soc* 133:8900–8902
- [6] Guang L, Hupp JT (2010) Metal-organic frameworks as sensors: a ZIF-8 based Fabry-Pérot device as a selective sensor for chemical vapors and gases. *J Am Chem Soc* 132:7832–7833
- [7] Wu X, Huang J, Cai W, Jaroniec M (2014) Force field for ZIF-8 flexible frameworks: atomistic simulation of adsorption, diffusion of pure gases as CH₄, H₂, CO₂ and N₂. *RSC Adv* 4:16503–16511
- [8] Bhattacharyya S, Pang SH, Dutzer MR et al (2016) Interactions of SO₂-containing acid gases with ZIF-8: structural changes and mechanistic investigations. *J Phys Chem C* 120:27221–27229
- [9] Xaver B, Bernd P, Lygia TB (2010) High frequency of fumigants and other toxic gases in imported freight containers—an underestimated occupational and community health risk. *Occup Environ Medicine* 67:207–212
- [10] Xiao JT, Yang B, Anh D et al (2009) Formaldehyde in China: production, consumption, exposure levels, and health effects. *Environ Int* 35:1210–1224
- [11] Jian FY, Dehua D, Dan L et al (2011) Contra-diffusion synthesis of ZIF-8 films on a polymer substrate. *Chem Commun* 47:2559–2561
- [12] Shamsaei E, Lin X, Low ZX et al (2016) Aqueous phase synthesis of ZIF-8 membrane with controllable location on an asymmetrically porous polymer substrate. *ACS Appl Mater Inter* 8:6236–6244
- [13] Zhang W, Chen L, Xu L et al (2019) Advanced nanonetwork-structured carbon materials for high-performance formaldehyde capture. *J Colloid Inter Sci* 537:562–568
- [14] Baur GB, Spring J, Kiwi-Minsker L (2018) Amine functionalized activated carbon fibers as effective structured adsorbents for formaldehyde removal. *Adsorption* 24:725–732
- [15] Lee KJ, Nanako S, Gang HL et al (2010) Activated carbon nanofiber produced from electrospun polyacrylonitrile nanofiber as a highly efficient formaldehyde adsorbent. *Carbon* 48:4248–4255
- [16] Suresh S, Bandosz TJ (2018) Removal of formaldehyde on carbon-based materials: a review of the recent approaches and findings. *Carbon* 137:207–221
- [17] Yan S, Qiao W, Yoon SH et al (2010) Removal of formaldehyde at low concentration using various activated carbon fibers. *J Appl Polym Sci* 106:2151–2157
- [18] Liu QS, Zheng T, Wang P et al (2010) Adsorption isotherm, kinetic and mechanism studies of some substituted phenols on activated carbon fibers. *Chem Eng J* 157:348–356
- [19] Zheng W, Zhong M, Lei C (2016) Coal-based granular activated carbon loaded with MnO₂ as an efficient adsorbent for removing formaldehyde from aqueous solution. *Desalin Water Treat* 57:13225–13235

- [20] Lee DT, Zhao J, Peterson GW, Parsons GN (2017) Catalytic “MOF-Cloth” formed via directed supramolecular assembly of UiO-66-NH₂ crystals on atomic layer deposition coated textiles for rapid degradation of chemical warfare agent simulants. *Chem Mater* 29:4894–4903
- [21] Zhao J, Gong B, Nunn WT et al (2015) Conformal and highly adsorptive metal-organic framework thin films via layer-by-layer growth on ALD-coated fiber mats. *J Mater Chem A* 3:1458–1464
- [22] Klet RC, Wang TC, Fernandez LE et al (2016) Synthetic access to atomically dispersed metals in metal-organic frameworks via a combined atomic-layer-deposition-in-MOF and Metal-Exchange approach. *Chem Mater* 28:1213–1219
- [23] Wang X, Sun M, Meng B et al (2016) Formation of continuous and highly permeable ZIF-8 membranes on porous alumina and zinc oxide hollow fibers. *Chem Commun* 52:13448–13451
- [24] Zhu QY, Tang X, Feng S, Zhong Z, Yao J, Yao Z (2019) ZIF-8@SiO₂ composite nanofiber membrane with bio-inspired spider web-like structure for efficient air pollution control. *J Membrane Sci* 581:252–261
- [25] Jung MJ, Ju WK, Ji SI et al (2009) Nitrogen and hydrogen adsorption of activated carbon fibers modified by fluorination. *J Ind Engin Chem* 15:410–414
- [26] Huang H, Ye D, Huang B, Wei Z (2008) Vanadium supported on viscose-based activated carbon fibers modified by oxygen plasma for the SCR of NO. *Catal Today* 139:100–108
- [27] Rong HQ, Liu ZY, Wu QL (2010) Formaldehyde removal by Rayon-based activated carbon fibers modified by P-aminobenzoic acid. *Cellulose* 17:205–214
- [28] Chen H, Tang M, Rui Z et al (2016) ZnO modified TiO₂ nanotube array supported Pt catalyst for HCHO removal under mild conditions. *Catal Today* 264:23–30
- [29] Cheng HE, Chen CC (2008) Morphological and photoelectrochemical properties of ALD TiO₂ films. *J Electrochem Soc* 155:D604–D607
- [30] Singh R, Bapat R, Qin L et al (2016) Atomic layer deposited (ALD) TiO₂ on fibrous nano-silica (KCC-1) for photocatalysis: nanoparticle formation and size quantization effect. *ACS Catal* 6:2770–2784
- [31] Pan YC, Liu YY, Zeng GF et al (2011) Rapid synthesis of zeolitic imidazolate framework-8 (ZIF-8) nanocrystals in an aqueous system. *Chem Commun* 47:2071–2073
- [32] Chen F, Xin L, Yang H et al (2016) A simple one-step approach to fabrication of highly hydrophobic silk fabrics. *Appl Surf Sci* 360:207–212
- [33] Su Z, Zhang M, Lu Z et al (2018) Functionalization of cellulose fiber by in situ growth of zeolitic imidazolate framework-8 (ZIF-8) nanocrystals for preparing a cellulose-based air filter with gas adsorption ability. *Cellulose* 25:1–12
- [34] Ming H, Yao J, Qi L et al (2014) Facile synthesis of zeolitic imidazolate framework-8 from a concentrated aqueous solution. *Micropor Mesopor Mater* 184:55–60
- [35] Pokhrel J, Bhorla N, Anastasiou S et al (2018) CO₂ adsorption behavior of amine-functionalized ZIF-8, graphene oxide, and ZIF-8/graphene oxide composites under dry and wet conditions. *Micropor Mesopor Mater* 267:53–67
- [36] Mohanty P, Chauhan I (2014) Immobilization of titania nanoparticles on the surface of cellulose fibres by a facile single step hydrothermal method and study of their photocatalytic and antibacterial activities. *RSC Adv* 4:57885–57890
- [37] Chauhan I, Aggrawal S, Mohanty P (2015) ZnO nanowire-immobilized paper matrices for visible light-induced antibacterial activity against *Escherichia coli*. *Environ Sci Nano* 2:273–279
- [38] Aggrawal S, Chauhan I, Mohanty P (2015) Immobilization of Bi₂O₃ nanoparticles on the cellulose fibers of paper matrices and investigation of its antibacterial activity against *E. coli* in visible light. *Mater Express* 5:429–436
- [39] Chen W, Qian X, An X (2015) In situ green preparation and antibacterial activity of copper-based metal-organic frameworks/cellulose fibers (HKUST-1/CF) composite. *Cellulose* 22:3789–3797
- [40] Yu L, Wang L, Sun X, Ye D (2018) Enhanced photocatalytic activity of rGO/TiO₂ for the decomposition of formaldehyde under visible light irradiation. *J Environ Sci* 73:138–146
- [41] Liang W, Jian L, Jin Y (2012) Photo-catalytic degradation of gaseous formaldehyde by TiO₂/UV, Ag/TiO₂/UV and Ce/TiO₂/UV. *Build Environ* 51:345–350
- [42] Zhang G, Sun Z, Duan Y et al (2017) Synthesis of nano-TiO₂/diatomite composite and its photocatalytic degradation of gaseous formaldehyde. *Appl Surf Sci* 412:105–112
- [43] Portela R, Jansson I, Suárez M, Villarreal B (2018) Natural silicate-TiO₂ hybrids for photocatalytic oxidation of formaldehyde in gas phase. *Chem Engin J* 310:560–570
- [44] He M, Ji J, Liu B, Huang H (2018) Reduced TiO₂ with tunable oxygen vacancies for catalytic oxidation of formaldehyde at room temperature. *Appl Surf Sci* 15:934–942
- [45] Na CJ, Yoo MJ, Tsang DCW, Kim HW, Kim KH (2019) High-performance materials for effective sorptive removal of formaldehyde in air. *J Hazard Mater* 366:452–465

Publisher's Note Springer Nature remains neutral with regard to jurisdictional claims in published maps and institutional affiliations.